BIOMEDICAL ENGINEERING

HIGH RESOLUTION ULTRASONIC VESSEL IMAGING AND REPEATABILITY OF BLOOD FLOW MODELING USING AN ULTRASOUND CONTRAST AGENT

MARY ELIZABETH LOVELESS

Thesis under the direction of Professor Thomas E. Yankeelov

Cancer is a complex and adaptable disease, and knowledge of the mechanisms that cause its progression is vital to creating and monitoring anti-cancer therapies. As a tumor grows beyond a few mm^3, blood vessels are recruited to provide additional nutrients in a process called angiogenesis. Some novel drug therapies specifically target this process, and the efficacy of these drugs can in principle be monitored by a technique called angiography. 3D angiography, a method of imaging the vasculature, can be performed by several imaging modalities typically with the use of a contrast agent.

A technique is introduced which uses high resolution ultrasound in conjunction with an ultrasound contrast agent to produce 3D images of the vasculature. This method offers a faster, more accessible, and cheaper alternative to assess the efficacy of anti-angiogenic drugs in preclinical cancer models. In addition to vessel imaging, modeling the kinetic behavior of the contrast agent in the vasculature can elucidate parameters such as blood flow, which can also serve as an indicator of drug treatment efficacy. The repeatability of a commonly used mono-exponential model is assessed in order to determine thresholds for inter/intra-subject error.

The 3D vessel imaging technique presented in this thesis correlated with other measures of blood flow ($r = 0.55 \pm 0.04$, $p < 0.01$) and shows an increased sensitivity to microvasculature within tumors. Also, preliminary repeatability analysis ($n = 6$) on the modeling parameter which is proportional to contrast agent velocity shows a mean difference of 0.061 ± 0.298 between independent measurements, and the limits of agreement range from -0.536 and 0.656. The developments exhibited provide additional methods for monitoring longitudinal anti-angiogenic cancer treatments in preclinical models.

Approved:

Professor Thomas E. Yankeelov

HIGH RESOLUTION ULTRASONIC VESSEL IMAGING AND REPEATABILITY OF BLOOD FLOW MODELING USING AN ULTRASOUND CONTRAST AGENT

By

Mary Elizabeth Loveless

Thesis

Submitted to the Faculty of the

Graduate School of Vanderbilt University

in partial fulfillment of the requirements

for the degree of

MASTER OF SCIENCE

in

Biomedical Engineering

December, 2007

Nashville, TN

Approved:

Professor Thomas E. Yankeelov

Professor John C. Gore

ACKNOWLEDGMENTS

I would like to thank my funding sources for their support during the investigation of this work. The National Institute of Health (NIH) pre-doctoral training grant (NIH 5 T32 EB003817), the American Institute of Ultrasound in Medicine (AIUM) Endowment for Education and Research grant, and the NIH/National Cancer Institute (NCI) U24 CA126588 grant generously provided the funding for materials and time to produce the work presented in this thesis.

I would also like give a huge thanks to those individuals that have contributed time and effort to this work. Specifically, I appreciate the efforts of Jessica Huamani and Dr. Dennis Hallahan for providing the animal models of cancer used to develop the methodology. To Dr. Xia Li and Dr. Benoit Dawant, I extend my gratitude for the help with imaging processing and registration. Dr. Andrej Lyshchik graciously gave his time in developing procedures to make this work possible. I thank Mr. Jarrod True for assistance for animal handling and Dr. Tuhin Sinha and Dr. Jeff Luci for analytical and technical consults. Thanks also go to Dr. Leena Choi who assisted in statistical analysis. To those members of the Vanderbilt Cancer Imaging Group (VCIG), I appreciate all the ideas and discussions to help progress this work. Last but certainly not least, I would like to thank Dr. John Gore and Dr. Thomas Yankeelov for their continued advice and support.

On a more specific note, a huge debt of gratitude is owed to my advisor Dr. Thomas Yankeelov. Not only was his knowledge and experience continually sought after during the development and analysis of the work presented here, but his sense of humor and

willingness to help at any time were invaluable. Many thanks go to him for providing an interesting and engaging learning environment. You're the coolest.

Saving the best for last, I would like to thank my husband, Daniel Loveless, who probably knows more about this work than he ever anticipated. He has provided not only enlightening discussions but moral support and patience throughout this whole process. This work would not have been possible without all his encouragement and understanding. And to my family, I thank you all for your patience and understanding. Your unconditional love provides the cornerstone for my success. Thanks to all of you; I would not be where I am today without you.

TABLE OF CONTENTS

LIST OF FIGURES

Figure Page

LIST OF TABLES

Table Page

CHAPTER I

INTRODUCTION

Cancer and Angiogenesis

While no single definition can characterize all forms of cancer, for the sake of simplicity, a usefule general definition of cancer is "a set of diseases characterized by unregulated cell growth leading to invasion of surrounding tissues and spread (metastasis) to other parts of the body" [1]. This definition is insufficient due to the many different types of cancers in existence (e.g., lung, breast, pancreas, skin melanoma, etc) that all express varying attributes that govern growth rate, metastatic state, and lethality. While prevention is the best defense against cancer, understanding the mechanisms responsible for the behaviors of various cancers can elucidate methods of early detection and treatment.

One specific characteristic of cancer that has been exploited for monitoring tumor growth and treatment response is angiogenesis. Angiogenesis is the recruitment of blood vessels by the primary cancer site in order to provide additional nutrients. As the tumor grows beyond approximately one mm^3, diffusion can no longer provide essential nutrients for the tumor cells thus creating hypoxic regions. Growth factors such as platelet-derived growth factor, fibroblast growth factor (FGF), and vascular endothelial growth factor (VEGF) are then secreted to promote the migration of endothelial cells to the site through a chemotactic response to the growth factor concentration [1]. However, the vessels produced differ from normal vasculature; the vessels are typically tortuous,

leaky, and poorly constructed. Thus, monitoring angiogenesis provides insight into tumor growth and anti-angiogenic treatment response [2-3].

Angiography

Imaging can provide a non-invasive means for examining the tumor microenvironment for both pre-clinical and clinical applications. Biopsies are invasive and challenging during longitudinal studies of cancer. Imaging provides non-invasive *in vivo* monitoring of the progression, growth and functionality of the cancer. Different imaging modalities provide methods of measuring angiogenesis *in vivo*; angiography, or the mapping of vasculature, is typically accomplished by the use of an exogenous contrast agent. In magnetic resonance imaging (MRI), a paramagnetic agent, such as gadolinium, is injected into the blood stream. The agent changes the relaxation time of the surrounding tissue and thereby affects the tissue contrast. In computed tomography (CT), iodine based contrast agent is typically used because of its ability to attenuate more X-rays than the surround tissue. However, these modalities have both strengths and weaknesses. While MRI uses non-ionizing radiation, the process can be time-consuming and costly. CT requires a dose of radiation for every visit so longitudinal studies are limited. This thesis presents a safe, cost-effective, and time-saving alternative to these methods using contrast enhanced ultrasound (CEUS) as a method for high resolution 3D vessel imaging in small animal models of cancer.

Ultrasound

Ultrasound imaging exploits the acoustic properties of tissue. The technique utilizes a transducer that transforms electrical energy into mechanical energy to produce a sound wave that can propagate through a medium (tissue). This longitudinal wave will cause elements of the medium to vibrate at individual velocities (*u(x,t)*). For a planar wave, the ratio of the acoustic pressure and the particle velocity (*u(x,t)*) is the acoustic impedance (*Z*) a characteristic of the medium. As the waves continue through the tissue, the energy can be absorbed, scattered or reflected back to the source. The sound wave obeys Snell's Law of Refraction:

$$Z_1 \sin(\theta_1) = Z_2 \sin(\theta_2) \qquad \textit{(Equation 1)}$$

where θ is the angle of incidence of the first medium and the angle of refraction within the second medium, and Z_1 and Z_2 are the acoustic impedances of the first and second media, respectively. The intensity of the reflected wave (*R*) at normal incidence depends on the change in *Z* of the tissue and incident intensity (*I*):

$$R = \left[\frac{Z_1 - Z_2}{Z_1 + Z_2}\right]^2 \cdot I \,. \qquad \textit{(Equation 2)}$$

The acoustic impedance depends on the density and elastic stiffness of the medium and varies between different biological tissues. Consequently, changes in Z produce backscattered ultrasound (echoes), and they are the basis of the contrast seen in ultrasound images.

Ultrasound Contrast Agents (UCAs)

According to *Equation 2*, the larger the difference in impedance between two sections of tissue, the more reflection occurs at the interface between those two media. UCAs are composed of air or high density gas surrounded by a stabilization shell [4-8] yielding an acoustic impedance value of approximately 0.0004 x 10^6 rayls while the *Z* value for blood is 1.65 x 10^6 rayls [9]. Delivering UCAs into the bloodstream creates a significant reflected signal that can indicate spatial information about where the contrast agent is distributed. As acoustic energy is deposited, the UCA begin to expand and contract at a certain frequency. The natural frequency or resonance frequency (f_0), at which the bubble oscillates is related to its radius (*r*):

$$f_0 = \frac{1}{2\pi r}\sqrt{\frac{3\gamma P_0}{\rho_0}} \qquad \textit{(Equation 3)}$$

where P_0 is ambient fluid pressure, γ is the adiabatic ideal gas constant, and ρ_0 is ambient fluid density [10].

For microbubbles with sizes less than 10 μm, the natural frequency falls within the diagnostic ultrasound range of 1 – 20 MHz. The increased reflectance of the resonating UCA is due to the expansion (followed by a contraction) of the bubble size. As shown in *Figure 1,* at low power input, the microbubbles behave in a linear fashion, resonating at the natural frequency. However, at higher power input, the contrast agent begins to demonstrate nonlinear resonance, producing harmonics of the natural frequency [10]. At even higher power, the bubbles can be destroyed by extreme expansion and contraction, which can be advantageous in some applications.

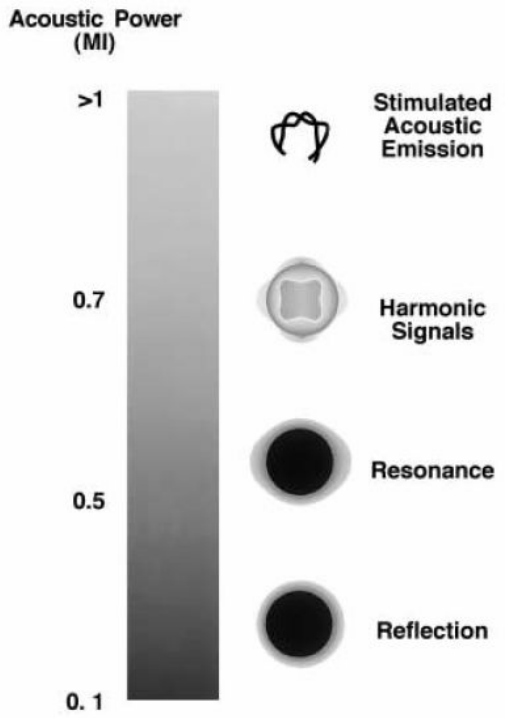

Figure 1. Microbubble behavior changes as a function acoustic power. As the mechanical index (MI) increases, the microbubbles oscillate at different frequencies until disruption [11].

Kinetic Modeling of Ultrasound Contrast Agents

In order to provide quantitative measurements with UCAs, two main assumptions are required. The first assumption requires that the UCA do not have a hemodynamic effect (i.e., no influence on blood flow or circulation) [12-13], and secondly, the UCAs are assumed to remain in constant flow and are not metabolized in any way [14]. With these assumptions, mathematical models have been produced to assess such properties as tissue blood flow, vascular integrity, branching pattern, and density using UCA [11,15-17].

Since UCAs can be destroyed at a high mechanical index (M.I.), imaging reperfusion of an area allows for repeated measurements of the contrast dynamics. After a certain time following a contrast agent infusion, the concentration of contrast reaches a steady-state within the blood. By destroying the microbubbles in a section of vasculature, the

replenishment of contrast agent can reflect cross sectional area, UCA velocity, and blood flow [17]. Plotting the time course before, during and after a bolus of contrast is injected or destruction sequence yields a time intensity curve (TIC) such as in *Figure 2*.

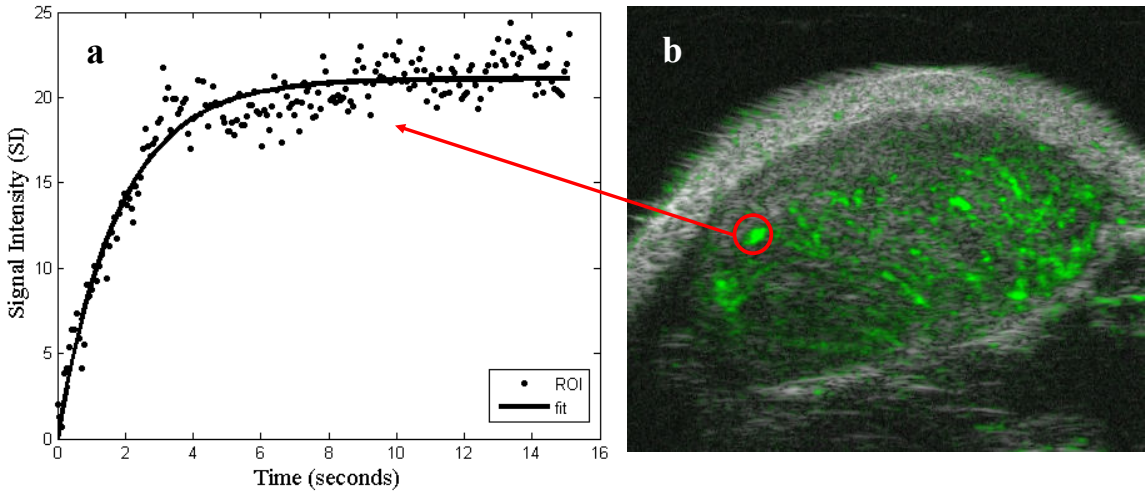

Figure 2. Panel a represents a time intensity curve produced from the region of interest (ROI) selected in panel b. Panel b is a B-mode image of a subcutaneous tumor in a mouse. The green overlay indicates the increased signal intensity from UCA. The signal intensity increases mono-exponentially as the UCA enters the field.

This TIC can be described mathematically by examining the shape of the curve produced with the following equation:

$$VI(t) = B \cdot [1 - \exp(-\beta \cdot t)], \qquad \textit{(Equation 4)}$$

where *VI(t)* is backscattered intensity at time *t*, *B* is the asymptotic plateau, and β is the rate of replenishment of microbubble concentration. For each pixel within an ultrasound image, the intensity changes based on the concentration of the agent present [12,18]. The curve is fit to *Equation 4* which provides parameters of *B* and β, estimates of vessel cross-sectional area and UCA velocity, respectively. The product of these two parameters provides an estimate of blood flow.

CHAPTER II

DEVELOPMENT OF HIGH RESOLUTION CONTRAST ENHANCED VESSEL IMAGING USING ULTRASOUND

Introduction

Non-invasive imaging methods that can quantitatively evaluate tumor microvasculature in pre-clinical models of cancer can provide valuable information on both tumor growth and treatment response. In particular, treatments that affect the vasculature of a tumor (e.g., anti-angiogenic drugs) can be monitored using vessel imaging techniques. Several imaging modalities can be used to generate 3D angiograms for monitoring vessel distribution and anti-angiogenic treatment effects, and each modality has both strengths and weakness. While CT techniques can approach resolutions on the order of 50 μm, each scan requires the use of ionizing radiation and injections of relatively large volumes (300-400 μL in mice) of contrast agent, thereby limiting the number of repeat studies that can be performed. Magnetic resonance angiography (MRA) requires no ionizing radiation and provides a spatial resolution of approximately 80 μm in reasonable time [19], but the technique is costly, time consuming, and not always reliable in the presence of physiological motion. Ultrasound methods have been proposed for vessel imaging by exploiting the Doppler effect. Changes in the frequency of the ultrasound signal caused by the movement of the flowing blood through static tissue allow Doppler ultrasound techniques to isolate vasculature. However, this type of analysis is known to have significant user-dependence. In particular, if the angle of the imaging plane is not perpendicular to the vessel, a true

cross-section of the vessel may not be measured thereby introducing significant errors [20]. Here we report our experience in imaging tumor vasculature using an alternative approach based on ultrasound contrast agents. UCAs provide a highly sensitive method of imaging microvasculature at the capillary level without the limitations of the above mentioned techniques [20].

As previously mentioned, UCAs are an intravascular contrast agent and can produce replenishment (wash-in) curves repeatedly during a single scan to characterize parameters such as blood flow in a particular area of interest [17]. These replenishment curves are time courses that characterize the intensity of the contrast produced as agent flows into a region of tissue and can be repeated by taking advantage of microbubble behavior under high power. By utilizing these characteristics, UCAs are attractive candidates for developing ultrasound contrast enhanced vessel imaging (CEVI), and their kinetic behavior can provide boundary parameters for the development of such a technique.

Once the UCAs are destroyed in a slice, the contrast agent reperfuses the region of interest. The image gathered immediately after the destruction pulse, which contains no contrast agent, can be subtracted from a later image that contains UCA to create an image that represents only the contrast enhanced vasculature. A 3D image of the vasculature can be created by incrementing through the tumor and repeatedly imaging the destruction and replenishment cycle in each slice. By examining how long the UCA remains in circulation as well as by obtaining the maximum number of destruction pulses that can be applied while maintaining significant enhancement, we develop a CEUS approach to generate high-resolution 3D images of tumor vasculature.

Materials and Methods

Data Acquisition

Duration of UCA Enhancement

All procedures adhered to our Institution's Animal Care and Use Committee guidelines. Eight female mice were injected subcutaneously with 10^6 67NR breast cancer cells in the hind limb. Eight days postinjection, they were imaged on a Visualsonics Vevo 770 (Toronto, Canada) system using a 40 MHz transducer mounted to a 3D motor on a rail system. Two days prior to imaging, 26G jugular catheters were surgically implanted for delivery of the contrast agent. During the imaging session, the animals were anesthetized with a 2%/98% isoflurane/oxygen mixture, and body temperature was monitored and maintained at 37^o C by a warming plate. Heart rate was also monitored and remained approximately 350 – 400 bpm.

Coupling gel was applied to the area of interest, and 2D B-mode and power Doppler scout images established a slice of tumor with vascularity present. The field of view varied from 9 mm X 9 mm to 12 mm X 12 mm depending on tumor size, establishing an in plane pixel size of less than or equal to ~25 μm X 25 μm. Image acquisition began immediately prior to a 50 μl bolus of Visualsonics Micromarker UCA (1.0 x 10^8 microbubbles/50 μL injection) injected *via* a jugular catheter. This UCA is specifically designed for high frequency (30 – 45 MHz) ultrasound imaging, and the diameter of the microbubbles range from 2 to 3 μm. Images were obtained within Visualsonics Contrast mode at a frame rate of 6-8 frames/second at 50% power (mechanical index (M.I.) of

0.14) for 10 minutes with no respiratory gating. This process was repeated for each mouse after 30 minutes which allowed for the clearance of any residual contrast [21].

Reperfusion repeatability

Animal preparation and field of view were identical to the duration of UCA enhancement study. Once the 50 μl bolus of Visualsonics Micromarker UCA injected reached steady state (approximately 45 seconds) [17,22], imaging began using the Visualsonics Contrast mode at a frame rate of 14 frames/second at 50% power. A 100% power destruction pulse (M.I. of 0.59) was administered, and images were collected for approximately 15-20 seconds in order to characterize the reperfusion curve. Twelve to eighteen sets of reperfusion images were collected using multiple destruction pulses over the maximum time dictated by the duration of UCA enhancement study described above. This process was then repeated for each subject after a 30 minute period of time.

3D CEVI

Using the preparation described in the previous studies, B-mode scout images established the most posterior slice of the region of interest. A 50 μl bolus of UCA was injected and allowed to reach equilibrium within the blood stream. Imaging at 50% power began after equilibrium was reached, and a destruction pulse was administered, followed by 15-20 seconds of image acquisition with no respiratory gating. Images were obtained within Visualsonics Contrast mode at a frame rate of 14 frames/second. The transducer was calibrated to fix on the next slice of tissue 330 μm in the anterior direction by manually incrementing a translation stage. A destruction pulse was administered followed by another 15-20 seconds of image acquisition. This process was repeated for each slice of tissue until the entire tumor was covered. Additional (up to three) injections

of UCA were utilized based on the maximum number of destructions determined in the reperfusion repeatability study described above.

3D power Doppler images were also obtained to compare the proposed vessel imaging method to an accepted ultrasound method of detecting flow. Using the same field of view and step size as the CEVI technique, 3D power Doppler and B-mode images of the tumor were also collected. Respiratory gating was used, and the power was set to 100% with the scan speed of 2.0 mm/s. The wall filter was set to 2.5 mm/s to eliminate echoes from the vessel wall movement.

Data Analysis

Duration of UCA Enhancement

Data analyses were performed using Visualsonics software, Microsoft Excel 2003 (Redmond, WA, USA), and Matlab R2006a (The Mathworks, Natick, MA, USA). ROIs of the entire tumor area were manually drawn, and the average intensity for each frame was computed in order to construct a time intensity curve for each mouse. Eight sets of TICs, two injections for each subject (one set), were exported to Excel, and the minimum intensity value was subtracted from all points in the time course to eliminate baseline noise. For each set, the TIC obtained from the first injection was plotted against the second injection TIC in order to assess the repeatability of the study. Additionally, each TIC was exported to Matlab to determine the time during washout in which enhancement from the UCA is no longer above 20% of the baseline during imaging.

Reperfusion repeatability

Data analyses were performed using Visualsonics software, Microsoft Excel 2003, and Matlab R2006a. ROIs of the entire tumor area were manually drawn, and the average intensity for each frame was computed in order to form a TIC for each subject. The data were then exported to Matlab. Each data segment containing a destruction pulse and subsequent reperfusion frames were separated into individual files, and the minimum intensity value was subtracted from all points in the time course. Time course data were smoothed temporally by using a moving window filter with a window size of three. Each time course for an injection contained anywhere from 12 to 18 segments.

3D CEVI

Data analyses were performed using Matlab R2006a. The maximum duration for UCA image enhancement and the number of destruction pulses allowed before insignificant enhancement were determined from the two studies described above, and the results were applied to determine data acquisition boundary parameters for 3D CEVI. The data were then exported to Matlab, and each frame within a time course was downsampled to a 256 X 256 image matrix. Frames within a data set were co-registered to the baseline time course frame using a rigid-body algorithm to eliminate any motion artifacts [23-24]. The registration algorithm relies on mutual information shared between each image set. A transformation is applied to the reference image that maximizes shared information with the target image file. The registered images were processed using a maximum intensity pixel (MIP) algorithm. The last slice was subtracted from the first post-destruction image to eliminate baseline intensity, and any pixel displaying intensity

less than 20% of the maximum was eliminated (i.e., set to zero intensity). In addition, a maximum change in intensity map was created. The mean and standard deviation were found from an ROI containing rapidly enhancing voxels, which are characteristic of the presence of an UCA. Any voxel below the mean of the ROI minus one standard deviation was not considered rapidly enhancing and was set to zero intensity. Finally, the images were filtered for stray pixels that had less than three enhancing pixels surrounding the pixel being interrogated. The process was repeated for each slice within a volume.

Processed CEVI slices and anatomical slices were fused into separate volume images. Anatomical volumes from the 3D CEVI region of interest were co-registered to anatomical volumes collected using the 3D power Doppler technique. The transformation was applied to the power Doppler data thereby registering it with the 3D CEVI data. Logical masks, where 1 represented vasculature signal and 0 represented no vasculature signal, were created for both the CEVI slice and the corresponding power Doppler slice in all data sets. 2D Pearson correlation coefficients for each slice were found using the `corr2` command in Matlab.

Results

Duration of UCA Enhancement

Time course images were obtained for each injection at an in plane pixel size of ~25 µm X 25 µm. ROIs were drawn and TICs were analyzed using this native resolution. Plots of the TIC were created in Excel, and visual inspection was used to predict the maximum clearance time of the UCA for the reperfusion repeatability study.

TABLE 1
Results from the Duration of UCA Enhancement Study

Mouse	Injection #	Time (min)	Slope	r	p-value
1	1 2	3.80 4.20	1.96	0.97	< 0.05
2	1 2	4.20 5.60	1.16	0.99	< 0.05
3	1 2	3.60 4.50	1.31	0.95	< 0.05
4	1 2	5.30 4.70	1.29	0.98	< 0.05
5	1 2	4.10 5.30	0.49	0.93	< 0.05
6	1 2	4.80 3.90	0.80	0.98	< 0.05
7	1 2	1.90 3.20	0.68	0.67	< 0.05
8	1 2	3.30 6.60	0.85	0.96	< 0.05

Table 1 presents the time each injection took to return to approximately 20% above baseline level. Baseline levels were described to be the average intensity immediately prior to contrast uptake. The mean time of UCA image enhancement was found to be 4.30 minutes $\pm$ of 1.09 minutes.

For each mouse, the TIC from injection one was plotted against the injection two TIC as demonstrated in *Figure 3*. Data were cropped such that it included only the wash out from each injection because possible variation in injection rate introduced unstable wash-in curves.

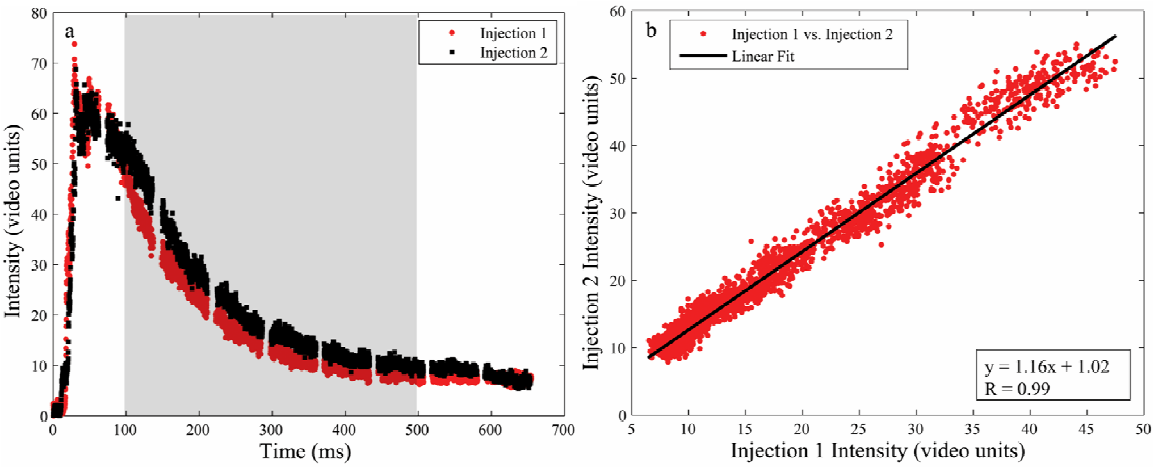

Figure 3. Panel a demonstrates the entire pre- and post-injection TIC with the highlighted region that was compared in panel b. The linearity seen in panel b depicts the repeatability of the washout curve.

Table 1 describes the slope and r-values corresponding to each set plotted. P-values for all sets of injections were computed using ANOVA and found to be less than 0.05 in all cases.

Reperfusion repeatability

Results were obtained from six mice; data from two mice were discarded due to errors in UCA injection; however, all eight mice were successfully used in the other studies described. Images produced were the same in plane resolution as described above. Time courses were exported to Excel to estimate the number of destructions

delivered before enhancement was insignificant. Example TICs resulting from this study are presented in *Figure 4*.

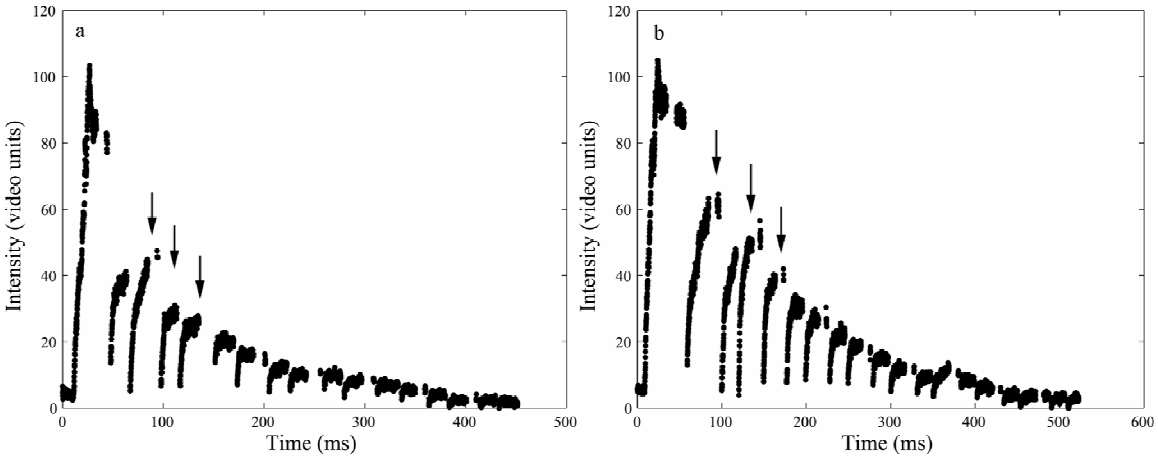

Figure 4. Panels a and b demonstrate two examples of multiple destructions applied to one slice of tissue. The arrows indicate several examples of the applied destruction pulse followed by the reperfusion of the UCA.

These estimated values were used during CEVI data acquisition to determine how many pulses can be administered and still maintain microbubble enhancement. Baseline levels were found for each injection, and the time after a destruction pulse was found where the maximum enhancement fell below 20% of the baseline. The number of destruction pulses were counted within that time and reported in *Table 2*. The average number of destructions was four pulses with a standard deviation of two pulses.

TABLE 2
Results from the Reperfusion Repeatability Study

Mouse	Injection #	# of Dest. Pulses
1	1	4
	2	7
2	1	4
	2	7
3	1	N/A
	2	N/A
4	1	N/A
	2	N/A
5	1	7
	2	6
6	1	1
	2	2
7	1	2
	2	4
8	1	5
	2	4

3D CEVI

Correlation coefficients for all slices were averaged and listed for each animal in *Table 3*.

TABLE 3
Results from the CEVI and Power Doppler ROI Correlation

Mouse	Average r value	Standard Deviation	Maximum r value	Minimum r value	p-value
1	0.603	0.058	0.676	0.413	< 0.01
2	0.535	0.086	0.674	0.372	< 0.01
3	0.594	0.081	0.784	0.448	< 0.01
4	0.511	0.056	0.616	0.373	< 0.01
5	0.524	0.069	0.642	0.385	< 0.01
6	0.508	0.085	0.665	0.285	< 0.01
7	0.52	0.148	0.729	0.179	< 0.01
8	0.602	0.096	0.717	0.314	< 0.01

By visually examining the data in a slice by slice manner, the CEVI and power Doppler data sets do noticeably correlate. The results in *Table 3* confirm this correlation indicating a mean $r = 0.55 \pm 0.04$ ($p < 0.01$). When the slices were overlaid and examined, such as in *Figure 5*, higher distributions of UCA seem to dominate the areas surrounding the vasculature mapped by power Doppler.

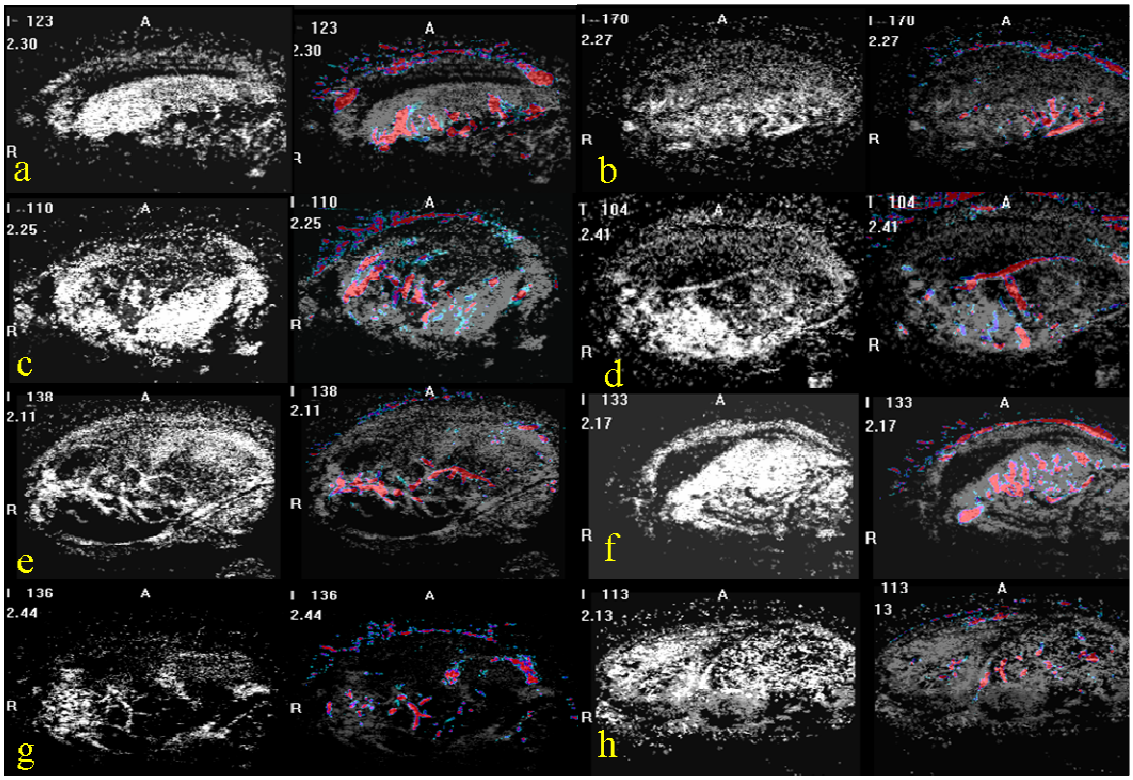

Figure 5. Panels a-h display a slice sets from each respective mouse. The left image in the set represents only the CEVI slice data while the rightmost image shows the power Doppler (red-blue data) overlaid on the matching CEVI slice. While the CEVI data corresponds with the power Doppler data, additional CEVI signal is visible surrounding most of the power Doppler signal that could be the results of CEVI having a higher sensitivity to the microvasculature.

In many slices, the CEVI data reveals additional vasculature or areas of higher perfusion that might have not been detected with power Doppler methods only. This phenomenon

is not unexpected since CEUS is known to be more sensitive than power Doppler to microvasculature at the capillary level [25]. *Figure 6* depicts the final reconstructed 3D CEVI volumes overlaid on the respective B-mode slices of each mouse.

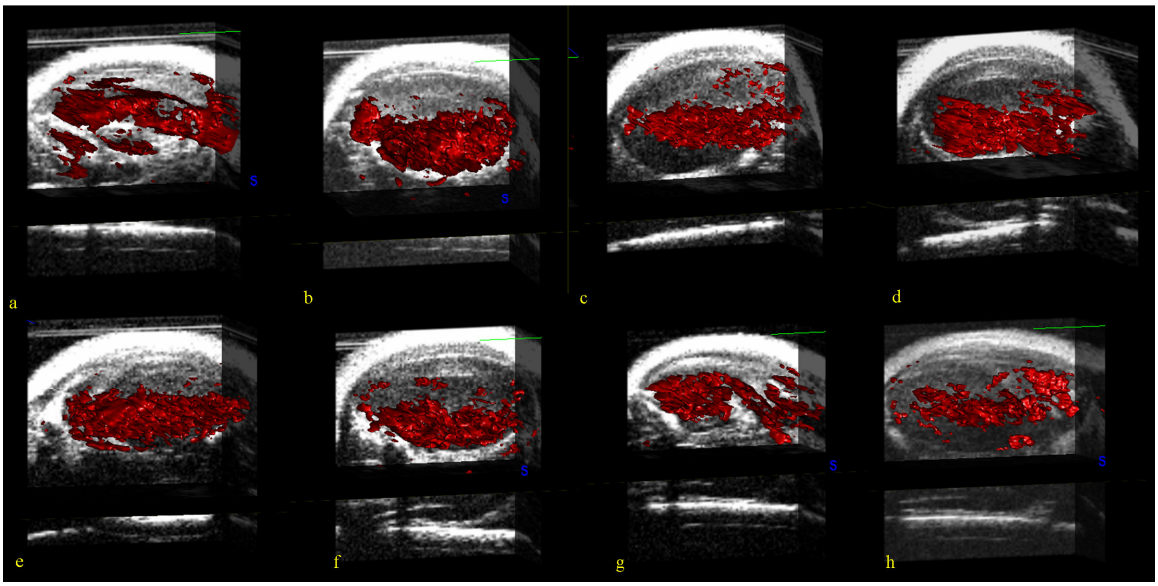

Figure 5. Panels a-h demonstrate the final 3D CEVI surface rendering overlaid on 3D B-mode slices for each mouse. A display filter isolated 80% of the signal and was applied such that vasculature from the skin would not be included in the 3D surface rendering. These 3D renderings provide spatial information about areas that are well-perfused within the tumor.

Discussion

The mean time of UCA image enhancement found in this study corresponds to values previously reported in the literature [26]. This parameter provides a temporal boundary for application in imaging studies involving UCAs. With a fixed 50% power applied, the washout curve appears reasonably consistent when repeated. In order to optimize repeatability, an automated syringe pump should be used in future studies. With an automated syringe pump both the amount of contrast injected as well as rate of injection are controlled across multiple injections and multiple subjects.

The reperfusion repeatability study provides the second essential boundary for developing a 3D CEVI technique. In order to isolate only contrast enhancement, a baseline image must be subtracted from each slice. This baseline image can be obtained by examining a slice absent of UCA; this state can be achieved by applying a destruction pulse. However, with each administered destruction pulse, a certain amount of UCA, which varies based on the vascularity of the ROI, are destroyed from circulation. This study has revealed an upper bound that is not only dependent on how long the UCA remains in circulation, but also how many destruction pulses can be administered until enhancement is not longer significant.

Upon visual inspection of the curves produced during this study, some data sets appeared to lose a significant percentage of enhancement after the first pulse while other data sets maintained an exponential decay of signal with each administered pulse. This observation could have been due to (at least) two factors. If a section of tissue was highly vascularized, a larger amount of the contrast could be destroyed, thereby reducing total enhancement of the entire tumor region. Another reason could be that the UCA did not reach steady-state in the blood stream. Care was taken to ensure that a pulse was not delivered until 45 seconds after injection, but if the UCA had not fully dispersed or the rate of injection was varied, the destruction of a large bolus could have affected the maximum number of pulses allotted to a volume of data.

The results of the 3D CEVI technique have shown potential for utilizing this technique for future vessel imaging related studies. While there does exist a noticeable correlation between CEVI and power Doppler, correlation is limited by the inherent flaws in the power Doppler measurement. The strong enhancement surrounding the power

Doppler signal could suggest the UCAs are more sensitive to the microvasculature surrounding or branching from primary vessels; this attribute has been noticed in previous reports [25,27]. While this finding needs to be confirmed with histology, it suggests that power Doppler is underestimating the extent of the vasculature while UCAs appear to be more sensitive to the vasculature neglected by the power Doppler measurement.

Multiple filters were applied to the collected data in order to isolate the contrast enhancement. Intra-slice registration aided in eliminating motion artifacts. Following the criteria from the reperfusion repeatability study, an intensity based filter was applied to the data in order to isolate all signal intensity higher than 20% of the maximum in the final MIP slice. However, during data acquisition a visual estimation of the number of destruction pulses allotted to one injection was found to be ~ 10 pulses. Only after quantitative analysis was this value found to be grossly overestimated, so slices imaged after the maximum number of destruction pulses may have lost significant contrast. This inherent issue might have increased the amount of signal being filtered during post-processing. Another filter was applied to eliminate spurious artifacts due to speckle. UCAs rapidly enhance intensity; so, by eliminating pixels that do not significantly change over time, other motion or speckle artifacts are removed. Finally, a filter was applied that isolated groups of enhancing pixels.

Automated rigid registration between the final volume sets provided a voxel by voxel comparison of the two data sets. However, interpolation between slices as well as errors during manual incremental stepping in the CEVI technique required adjustment of initial parameters, making the applied registration semi-automated. Utilizing a motor with a

fixed step size in future studies would eliminate registration issues due to errors in stepping between slices.

While this work demonstrates promising preliminary results, limitations in this study require future work. Refining methods of isolating the ultrasound contrast signal is necessary to provide more quantifiable results. Tracking the change in intensity not just temporally but spatially may provide very specific borders within the microvasculature. In addition, further studies are needed to validate this technique to other accepted angiography methods such as MRA or CT. Since UCAs can be targeted to specific intravascular receptors, this approach could be applied in constructing 3D representations of receptor distribution to further elucidate other molecular properties of the tumor involved in cancer progression [26,28].

To the best of our knowledge, the 3D CEVI approach presented here is the first attempt at a high resolution 3D vessel imaging technique using ultrasound contrast agents. This method provides a fast and accessible way of determining the progression of tumor growth or therapeutic efficacy of anti-angiogenic drugs. In addition, this technique allows ultrasound to become a 3D molecular imaging modality with the use of targeted ultrasound contrast agents. These advances presented further enable ultrasound to move from a structural imaging technique to a functional and molecular approach for quantitative cancer imaging.

CHAPTER III

REPEATABILITY OF BLOOD FLOW MODELING USING CONTRAST ENHANCED SONOGRAPHY

Introduction

The quantification of tissue function has become an important element in assessing tumor growth and cancer treatment efficacy. As treatments target specific aspects of the cancer, qualitative evaluation is no longer adequate in determining the value of a treatment option. For example, methods are needed to assess blood flow and tissue perfusion for drugs that target the tumor vasculature (i.e., anti-angiogenic treatments). Contrast agents have been used to exploit functional elements of the tumor milieu such as blood flow, pH, and matrix metalloprotease (MMP) activity in an array of different imaging modalities [29-36]. Some parameters, such as blood flow, have been measured using multiple modalities, including CEUS [17]. Relative to the other methods such as dynamic contrast enhanced magnetic resonance imaging (DCE-MRI) or contrast enhanced computed tomography (CT), CEUS presents a fast, cost effective, and safe option.

While many models exploit the kinetic behavior of UCAs to extract information about blood flow and vascularity, the model used in this study has been modified to examine blood flow in high frequency, high resolution CEUS [37]. High resolution CEUS has a lower signal to noise per voxel due to less UCA within an ROI. Therefore, TICs obtained from high resolution CEUS tend to be noisy and difficult to fit accurately.

Described below is the model used in this study; a more detailed description is available by Yeh, et al [37].

Adapted from Wei, et al [17], the reperfusion curve can be fit to a mono-exponential model described previously:

$$R(t) = A + (B - A)(1 - e^{-\beta t}), \qquad \textit{(Equation 4)}$$

where A represents intensity immediately after the destruction pulse (background intensity), B represents the steady-state intensity after contrast equilibration and β is a rate constant proportional to contrast velocity. If the image obtained immediately after the destruction pulse is subtracted from the subsequent reperfusion images,

$$A = 0$$

so that

$$R(t) = B * (1 - e^{-\beta t}). \qquad \textit{(Equation 5)}$$

In order to reduce parametric sensitivity to local noise error, a running average of the time intensity curve is utilized by integrating both sides and dividing by the time:

$$\frac{\int_0^t R(\tau)\,d\tau}{t} = \frac{B}{\beta t}(e^{-\beta t} - 1) + B \qquad \textit{(Equation 6)}$$

For each pixel, the integrative TIC (ITIC) can be fit to *Equation 6* to form maps of β, B, and $\beta \cdot B$, the latter has been shown to indicate blood flow [17,37]. For multiple destruction pulses on the same section of tissue, the β maps are expected to be equal until the UCA is destroyed and intensity returns to baseline. This study presents preliminary results regarding the repeatability of β measures for approximately five pulses produced from two separate injections in six mice.

Materials and Methods

Data Acquisition

All procedures adhered to our Institution's Animal Care and Use Committee guidelines. Eight female mice were injected subcutaneously with 10^6 67NR breast cancer cells in the hind limb. Eight days postinjection, they were imaged on a Visualsonics Vevo 770 (Toronto, Canada) system using a 30 MHz transducer mounted to a 3D motor on a rail system. Two days prior to imaging, jugular catheters were surgically implanted for delivery of the contrast agent. During the imaging session, the animals were anesthetized with a 2%/98% isoflurane/oxygen mixture, and body temperature was monitored and maintained at 37^o C by a warming plate. Heart rate was also monitored and remained approximately 350 – 400 bpm.

Coupling gel was applied to the area of interest, and 2D B-mode and power Doppler scout images established a slice of tumor with moderate vascularity. The field of view varied from 9 mm X 9 mm to 12 mm X 12 mm depending on tumor size, establishing an in plane pixel size of less than or equal to ~25 μm X 25 μm. Image acquisition began immediately prior to a 50 μl bolus of Visualsonics Micromarker microbubbles injected *via* a jugular catheter. These microbubbles are specifically designed for high frequency (30 – 45 MHz) ultrasound imaging, and the diameter of the microbubbles range from 2 to 3 μm. Once the 50 μl bolus of Visualsonics Micromarker microbubbles injected reached steady state (approximately 45 seconds) [11,27], imaging began using the Visualsonics Contrast mode at a frame rate of 14 frames/second at 50% power (mechanical index (M.I.) of 0.14) . A 100% power destruction pulse (M.I. of 0.59) was administered, and images were collected for approximately 15-20 seconds in order to characterize the

reperfusion curve. Twelve to eighteen sets of reperfusion images were collected using multiple destruction pulses over ten minutes. This process was then repeated for each subject after a 30 minute period of time to allow for clearance of residual contrast agent.

Data Analysis

From a previous study, it was found that approximately four ± two destruction pulses can be administered before the enhancement due to the UCA becomes insignificant. Using this finding as a guide, five sets of reperfusion data from each mouse and each injection were used to examine the repeatability of the parameters produced from *Equation 6*. Using the Visualsonics (Toronto, Canada) Vevo 770 software, ROIs were manually drawn around the entire tumor and TICs were exported to Matlab (The Mathworks, Natick, MA, USA) for each injection on each mouse. A Matlab algorithm fit the data to *Equation 6* using the command `lsqcurvefit`. Fit parameters were then exported to Matlab for statistical analysis.

For each injection for each mouse, B and β were plotted for five destruction pulses. The five β measurements were averaged for each injection for each subject, and Bland Altman plots were created using the differences between the averages for each injection [38].

Results

Plots of both the B and β parameters, as in *Figures 7 and 8*, reveal significant variation between subsequent destruction pulses. B appears to rely on the concentration

of the UCA in circulation and was not tested for repeatability. However, it is noted that it follows the general exponential decay of UCA seen in the *Figure 3*.

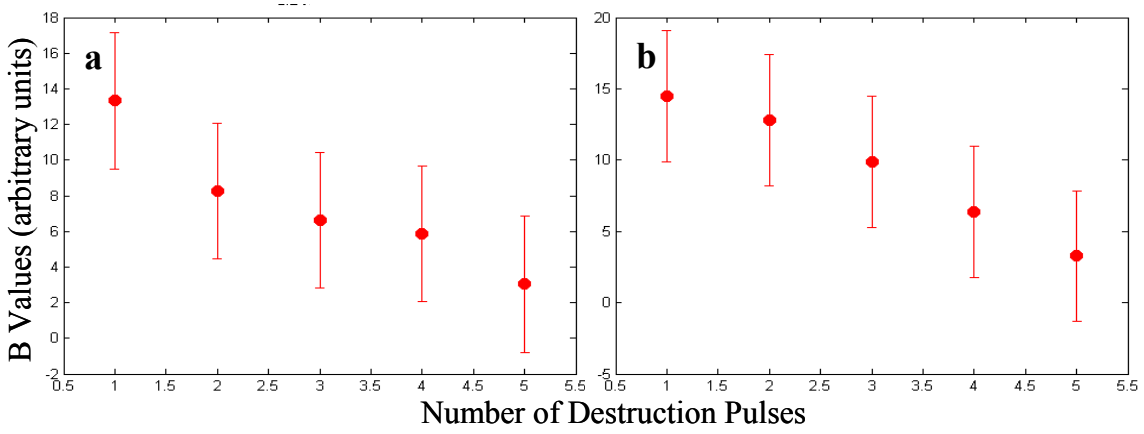

Figure 7. Five B parameters for one mouse with panel a shows the measurements for injection 1 while panel b plots injection 2. The error bars represent 1 standard deviation.

The β parameter was plotted and assessed for repeatability, and a Bland Altman plot is shown in *Figure 9*.

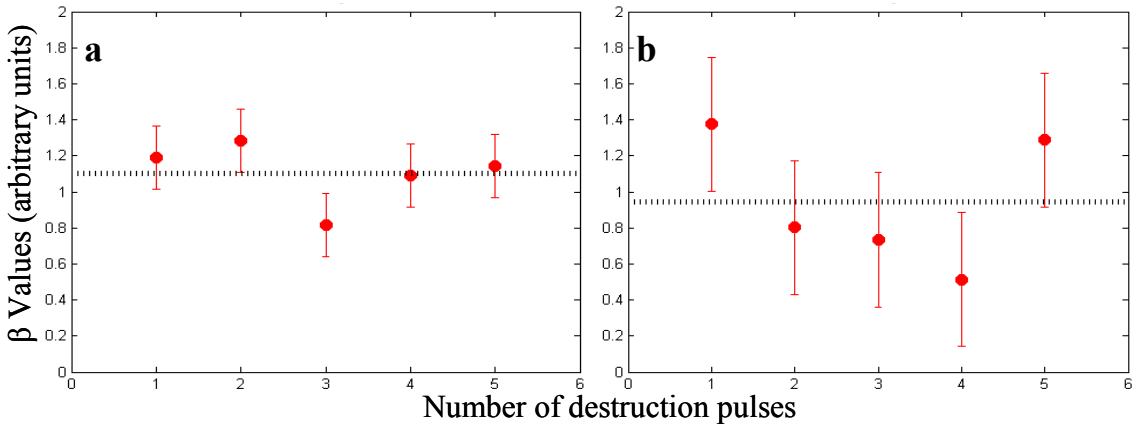

Figure 8. Five β parameters for one mouse with panel a showing the measurements for injection 1 while panel b plots injection 2. The dotted line represents the mean β value for the sample while the error bars represent 1 standard deviation of error.

The mean difference between the average β for each injection was found to be 0.061 ± 0.2980. The 95% lines of agreement fall on 0.656 and -0.536; thus, differences between injections for each animal would be expected to fall between these values with 95% confidence

.

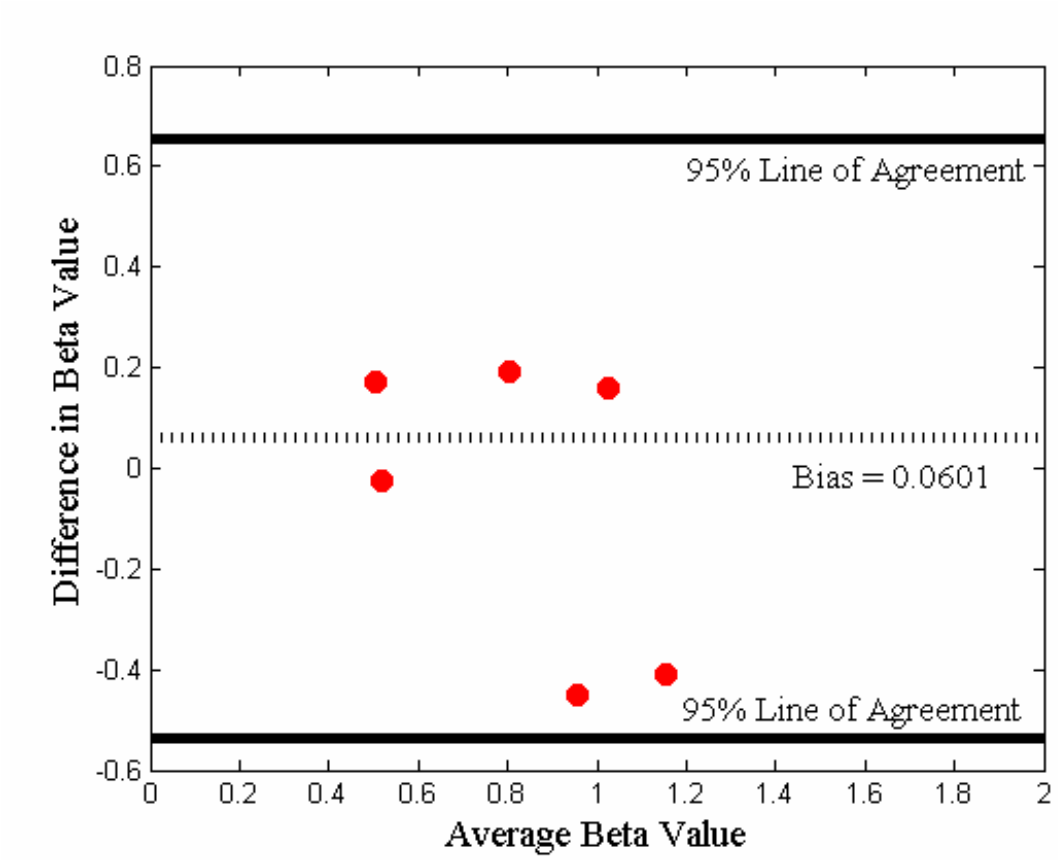

Figure 9. Bland Altman plot of the six mice. The dotted line represents the mean difference between injections on the same animal while the solid lines represent the 95% confidence interval.

Discussion

Upon initial interrogation into the variation among subsequent fit parameters, it was concluded that a repeatability assessment of the model must be performed. Theory regarding the model suggests that the β parameter, proportional to contrast velocity,

should change minimally throughout multiple destruction pulses. Although more subjects are needed to conclude the threshold for inter-/intra-subject error over repeated measurements, it is clear by the 95% range in *Figure 9* that the β parameter seems to have a greater fluctuation than anticipated for multiple measurements of the same section of tissue.

Some of the variation could be due to errors during acquisition. The UCA was injected *via* a jugular catheter manually over a 15 second interval and 45 seconds elapsed until the first destruction in order for the UCA to reach equilibrium in circulation. However, an automated syringe could have facilitated a more constant infusion rate, leading to a higher probability of the UCA reaching steady-state after the 45 second period of time post-injection. If steady state was not reached, a bolus of UCA could have been problematic when fitting to a model that assumes uniform distribution; thus, false or incorrect fit parameters could have introduced error in this study. As discussed previously, contrast-enhanced high frequency ultrasound imaging suffers from a lower signal to noise ratio (SNR). This lower SNR reflects less CA per voxel because of the increased spatial resolution. While using a model that eliminates much of the noise by integrating the signal over time provides better model fits, we can not assume that noise does not affect the output parameters. Thus, the low SNR could also affect the discrepancies in parametric repeatability. Tumor vasculature is inherently leaky and poorly constructed. These physiological variations could contribute to the disparity in parameter measurements as well.

This study has shown the preliminary findings that suggest poor repeatability of a clinically accepted method of blood flow modeling. In future studies, six more mice will

be incorporated into this study in order to determine a more adequate assessment. Further analysis will be used to determine the sources for any differences in kinetic modeling of the tumor microvasculature using high-resolution US imaging.

CHAPTER IV

CONCLUSIONS

This thesis has demonstrated a novel technique in monitoring tumor growth and anti-angiogenic cancer treatments. High resolution contrast enhanced vessel imaging is safe and cost-effective alternative to other 3D angiography techniques and provides higher sensitivity about vascularity and perfusion than current ultrasound blood flow measures.

While this technique shows promise, some limitations require additional study. First and foremost, methods in UCA tracking must be explored. Current filtering techniques need to be expanded to include a tracking algorithm that will examine both temporal and spatial changes in image intensity to further determine the UCA patterns. Developing a technique such as UCA tracking could provide better boundaries for microvasculature and reduce artifacts from motion.

The development of targeted microbubbles enables ultrasound to provide information about a region of tissue on a molecular level. For example, by targeting UCAs to VEGF receptors 1 and 2 (VEGF R1 and VEGF R2), molecular information can be obtained regarding the distribution of these receptors within tumors. This 2D methodology has been used to examine the efficacy of antiangiogenic and cytotoxic drugs in pancreatic cancer mouse models [39-40]. However, by using similar techniques as the 3D CEVI technique described, 3D molecular imaging can be achieved using ultrasound. 3D information regarding VEGF receptor distribution could not only provide additional insight to monitoring tumor growth and cancer treatments, but could also be integrated

into multi-parametric studies to assess many aspects of the same tumor over a long period of time.

In addition, preliminary results from the repeatability study of the commonly used mono-exponential model show greater change in values than anticipated. While more subjects are necessary to absolutely conclude the repeatability of this model, these initial findings allude to re-examination of the model when measuring microvascular blood flow.

This study has provided a reasonable alternative to other methods of angiography as well as a potential method for creating 3D representations of endothelial proteins; thus ultrasound has become a candidate for multi-modal and multi-parametric studies of the tumor microenvironment.

APPENDIX

ADDITIONAL FIGURES

Duration of UCA Enhancement plots for the 7 other subjects.

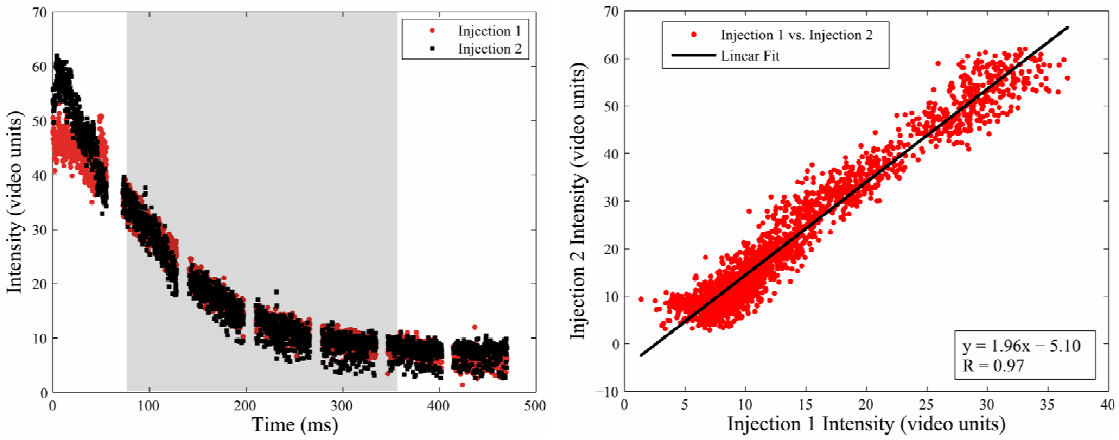

Figure 10. Time intensity curves from the duration of UCA enhancement study for Mouse 1. Panel a demonstrates the entire pre- and post-injection TIC with the highlighted region that was compared in panel b. The linearity seen in panel b depicts the repeatability of the washout curve.

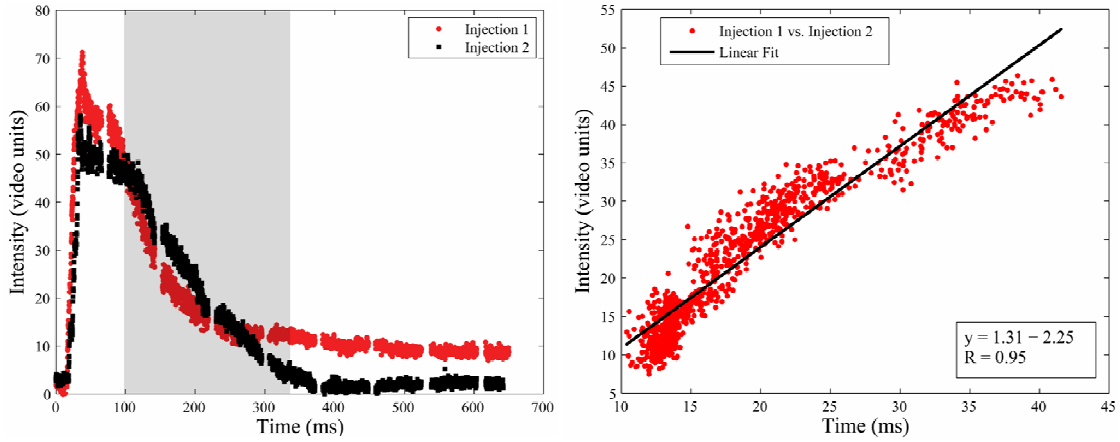

Figure 11. Time intensity curves from the duration of UCA enhancement study for Mouse 3. Panel a demonstrates the entire pre- and post-injection TIC with the highlighted region that was compared in panel b. The linearity seen in panel b depicts the repeatability of the washout curve.

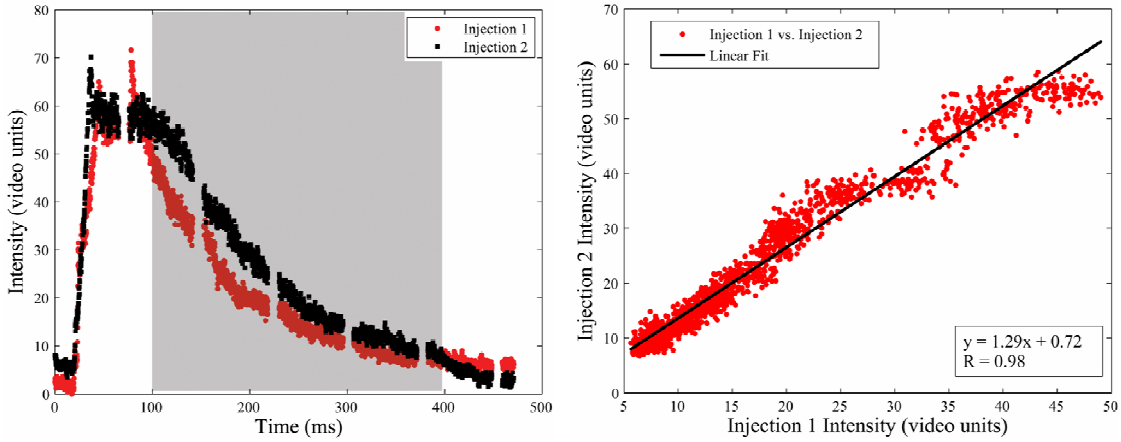

Figure 12. Time intensity curves from the duration of UCA enhancement study for Mouse 4. Panel a demonstrates the entire pre- and post-injection TIC with the highlighted region that was compared in panel b. The linearity seen in panel b depicts the repeatability of the washout curve.

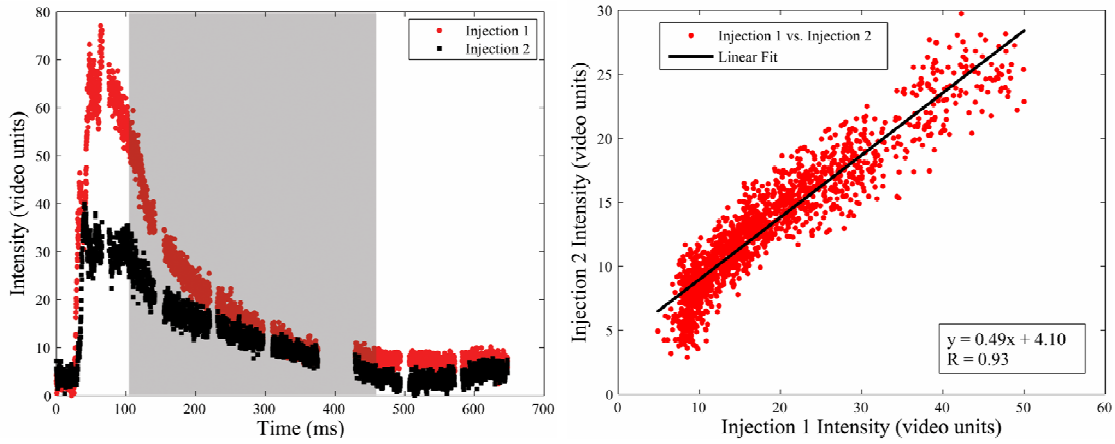

Figure 13. Time intensity curves from the duration of UCA enhancement study for Mouse 5. Panel a demonstrates the entire pre- and post-injection TIC with the highlighted region that was compared in panel b. The linearity seen in panel b depicts the repeatability of the washout curve.

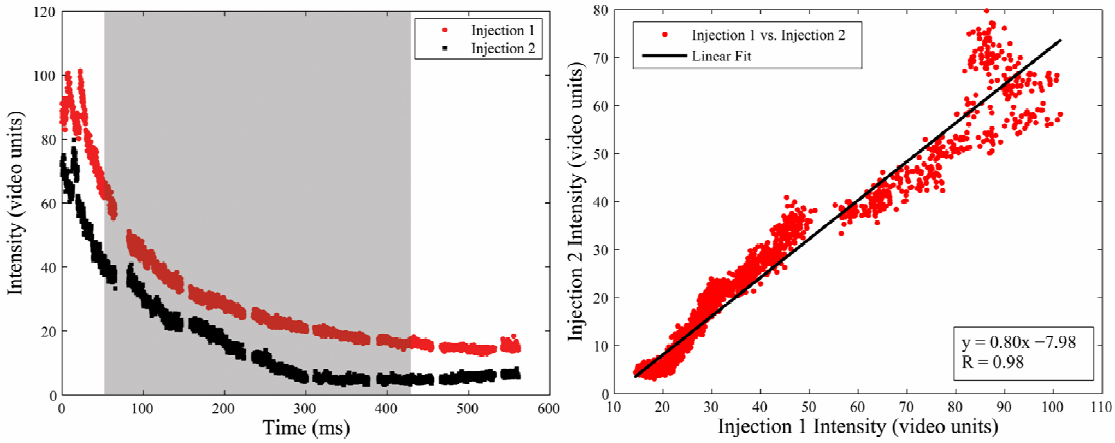

Figure 14. Time intensity curves from the duration of UCA enhancement study for Mouse 6. Panel a demonstrates the entire pre- and post-injection TIC with the highlighted region that was compared in panel b. The linearity seen in panel b depicts the repeatability of the washout curve.

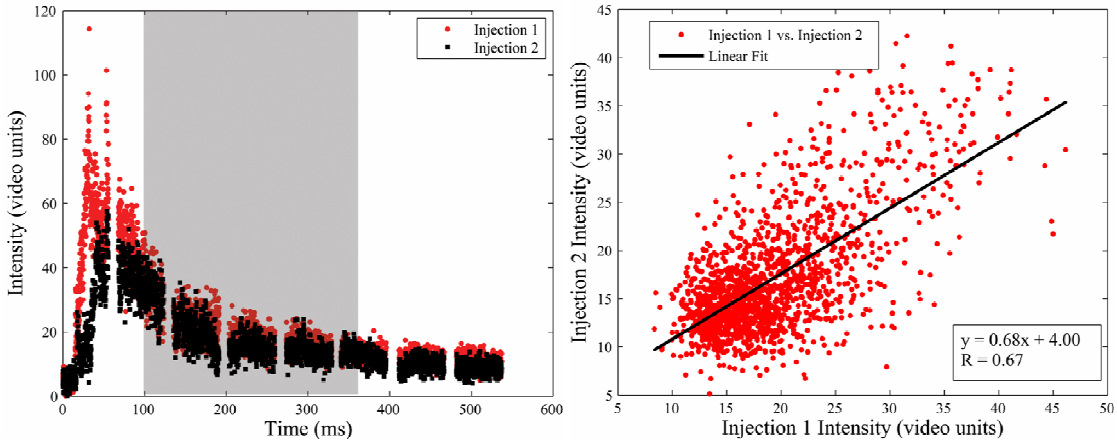

Figure 15. Time intensity curves from the duration of UCA enhancement study for Mouse 7. Panel a demonstrates the entire pre- and post-injection TIC with the highlighted region that was compared in panel b. The linearity seen in panel b depicts the repeatability of the washout curve.

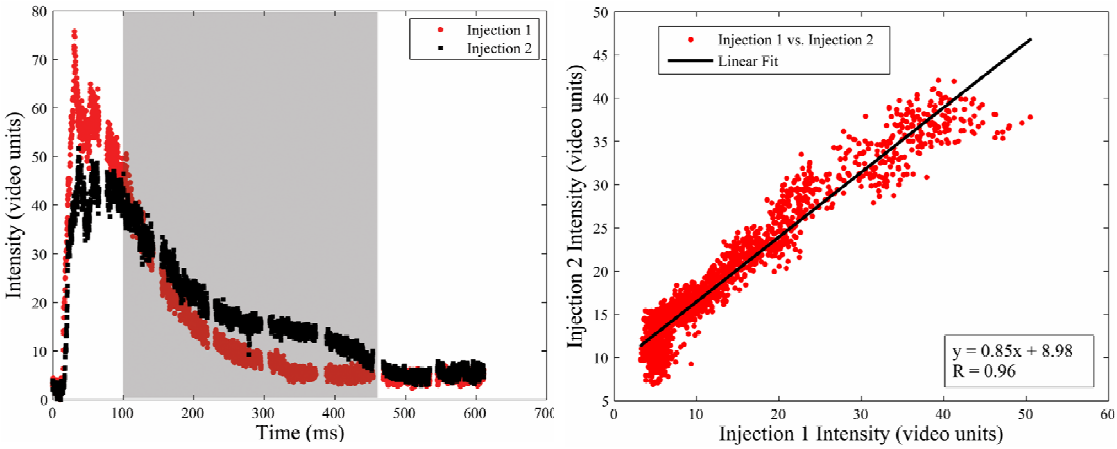

Figure 16. Time intensity curves from the duration of UCA enhancement study for Mouse 8. Panel a demonstrates the entire pre- and post-injection TIC with the highlighted region that was compared in panel b. The linearity seen in panel b depicts the repeatability of the washout curve.

Reperfusion repeatability plots for the 6 other subjects; however, mouse 3 was not used in study due to the lack of UCA enhancement and the data taken from mouse 4 was corrupted.

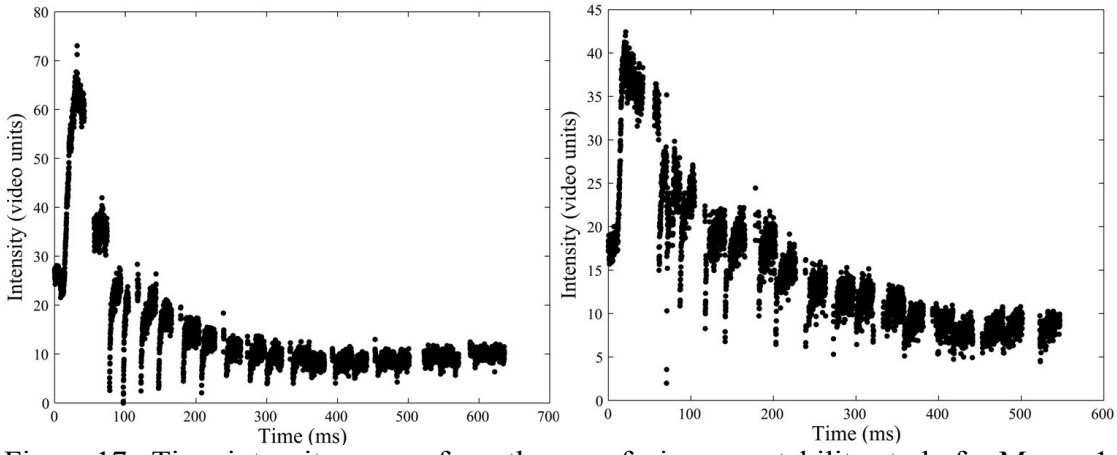

Figure 17. Time intensity curves from the reperfusion repeatability study for Mouse 1. Multiple destruction pulses were administered followed by imaging of the reperfusion of the contrast into the field of view. These figures show the intensity of the image increases after the destruction pulse destroyed all contrast.

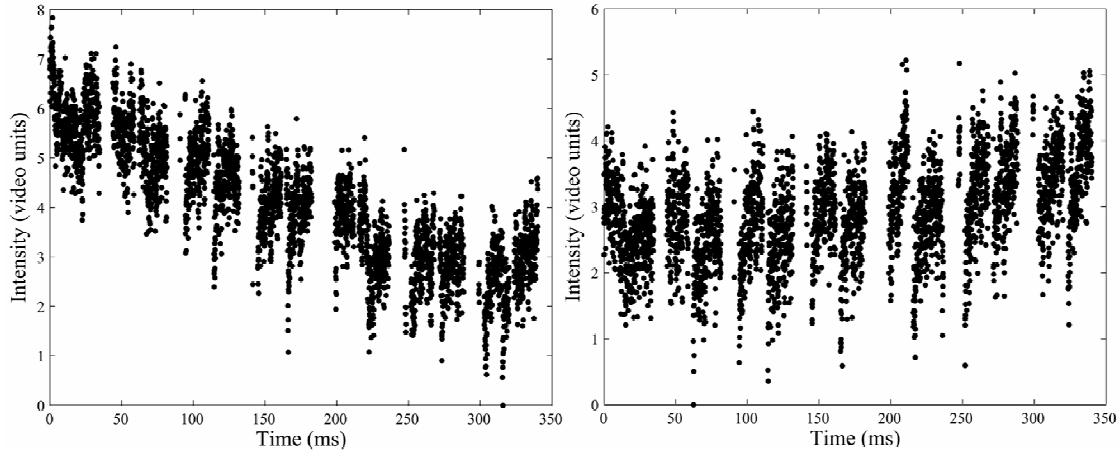

Figure 18. Time intensity curves from the reperfusion repeatability study for Mouse 3. Multiple destruction pulses were administered followed by imaging of the reperfusion of the contrast into the field of view. These figures show the intensity of the image increases after the destruction pulse destroyed all contrast.

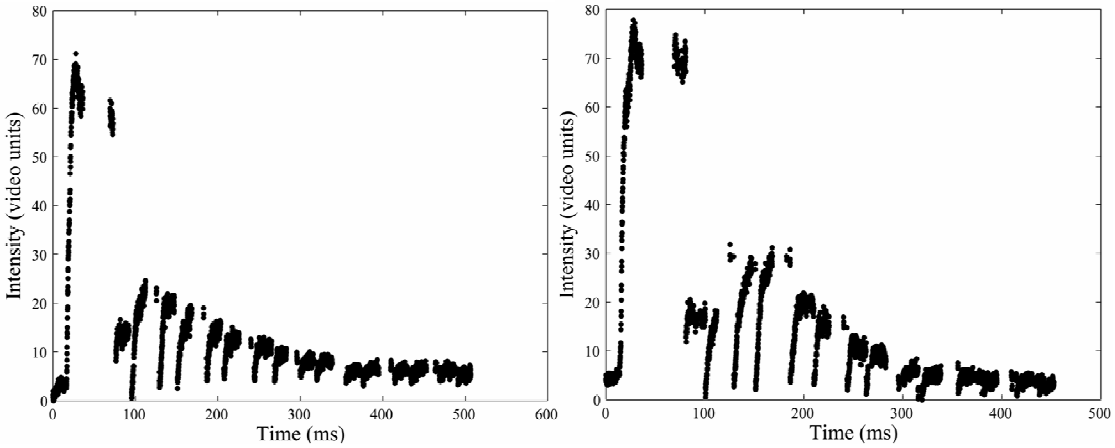

Figure 19. Time intensity curves from the reperfusion repeatability study for Mouse 5.

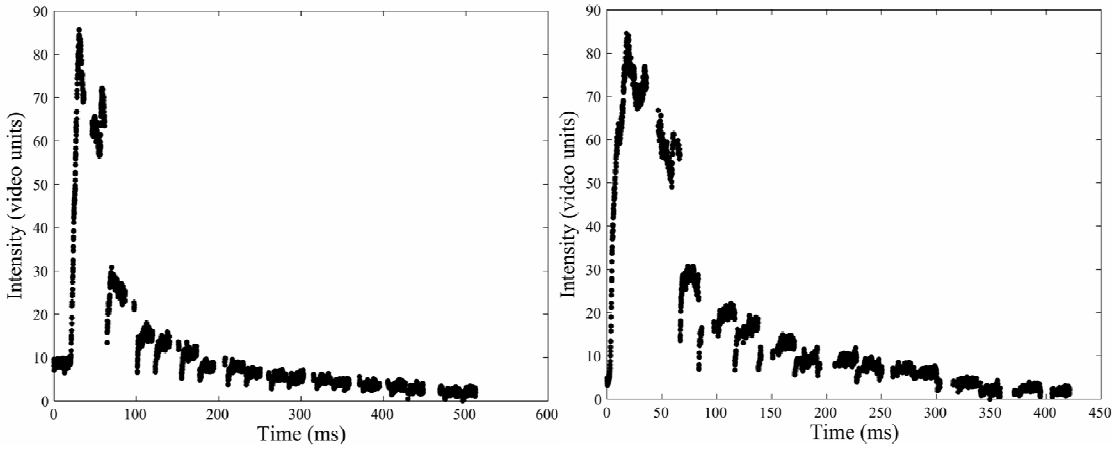

Figure 20. Time intensity curves from the reperfusion repeatability study for Mouse 6. Multiple destruction pulses were administered followed by imaging of the reperfusion of the contrast into the field of view. These figures show the intensity of the image increases after the destruction pulse destroyed all contrast.

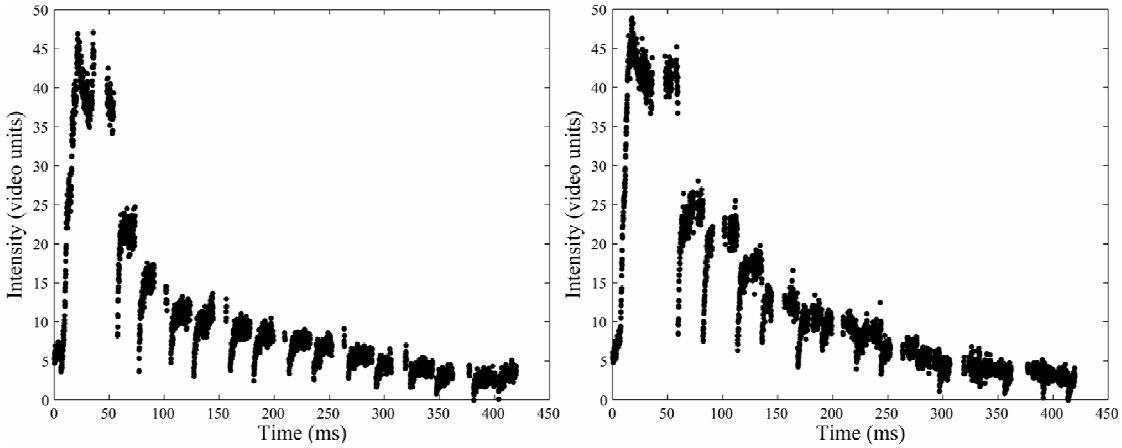

Figure 21. Time intensity curves from the reperfusion repeatability study for Mouse 7. Multiple destruction pulses were administered followed by imaging of the reperfusion of the contrast into the field of view. These figures show the intensity of the image increases after the destruction pulse destroyed all contrast.

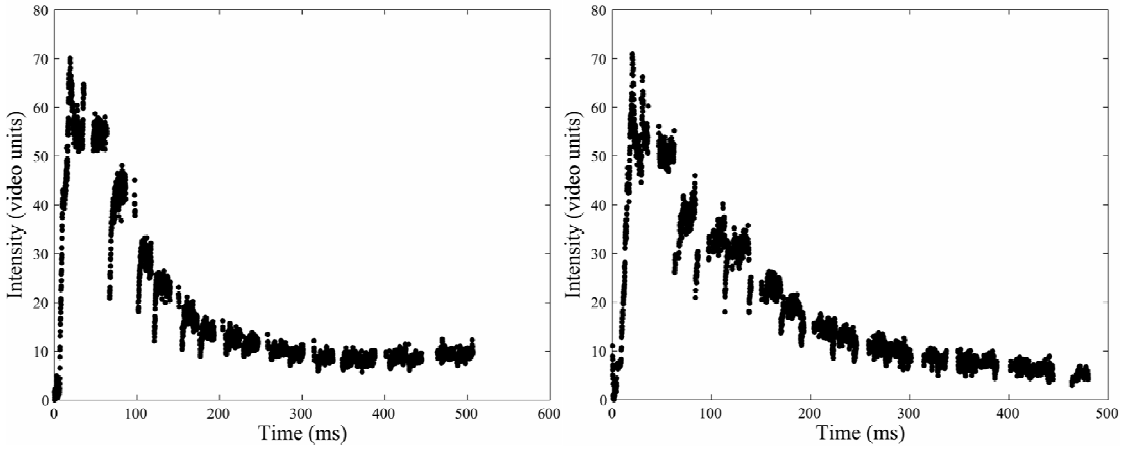

Figure 22. Time intensity curves from the reperfusion repeatability study for Mouse 8. Multiple destruction pulses were administered followed by imaging of the reperfusion of the contrast into the field of view. These figures show the intensity of the image increases after the destruction pulse destroyed all contrast.

Additional plots of the kinetic parameters derived from the blood flow modeling.

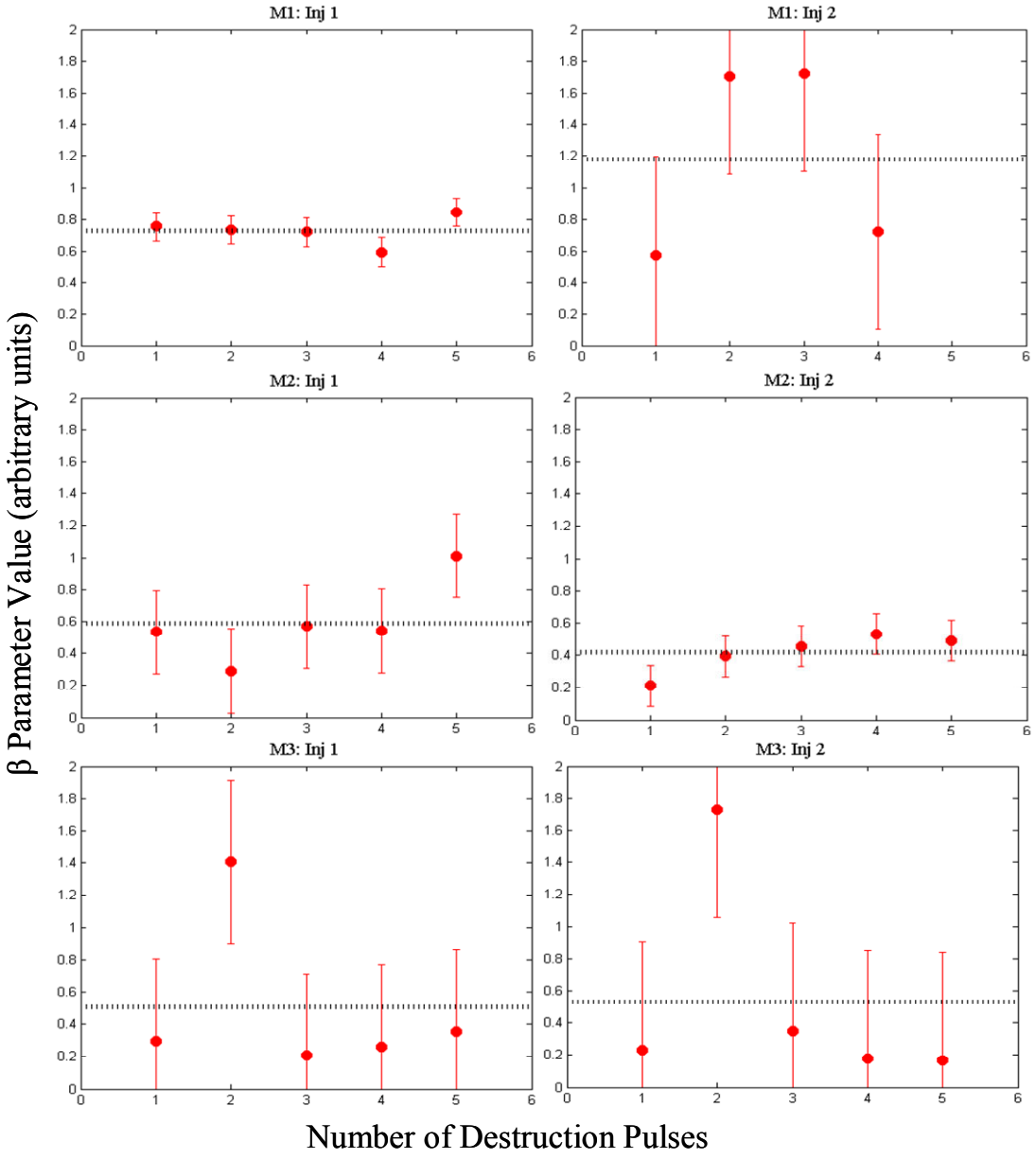

Figure 23. Five β measurements for each injection on mice 1-3. Error bars represent 1 standard deviation while the dotted line is the β value

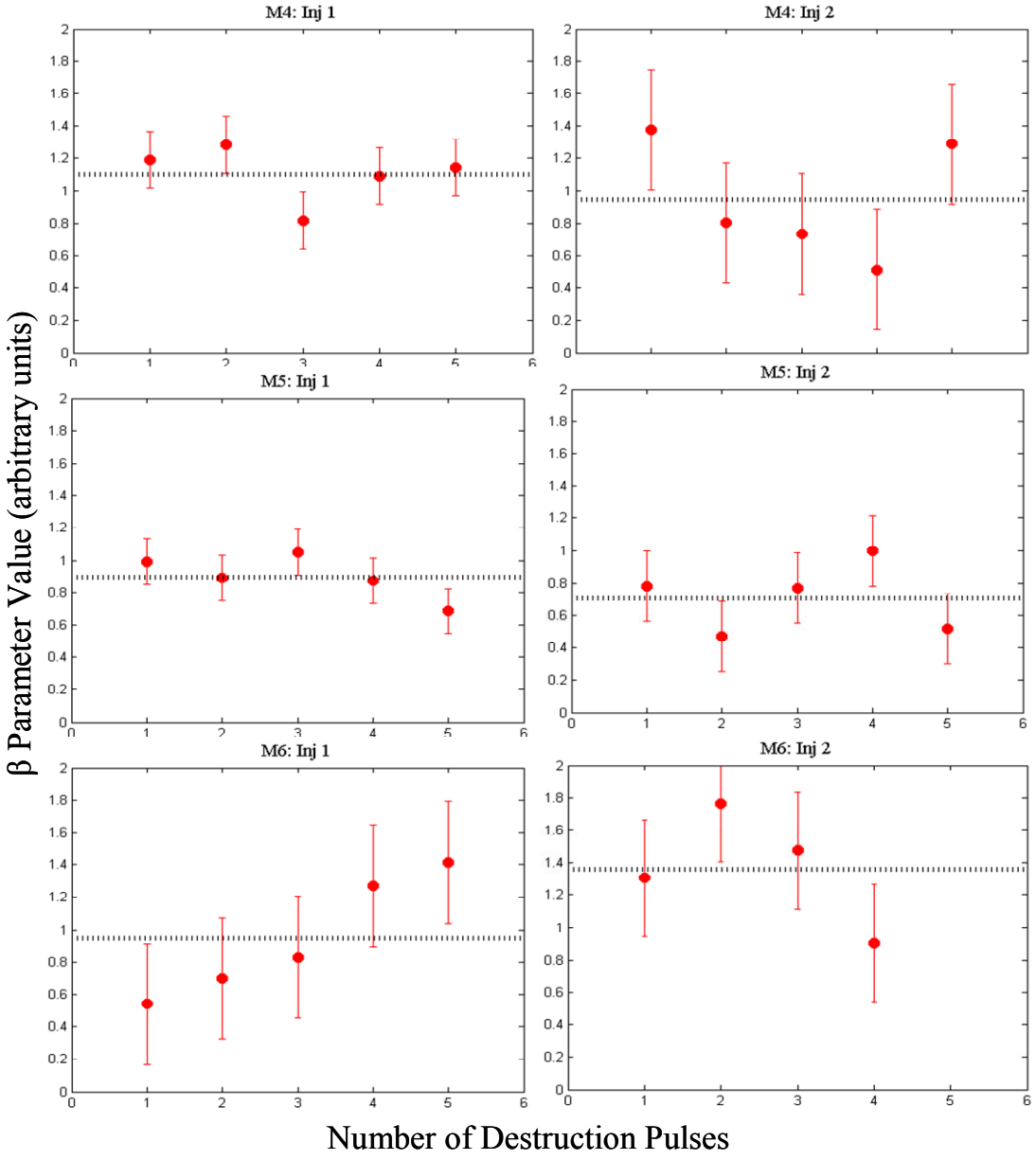

Figure 24. Five β measurements for each injection on mice 4-6. Error bars represent 1 standard deviation while the dotted line is the β value.

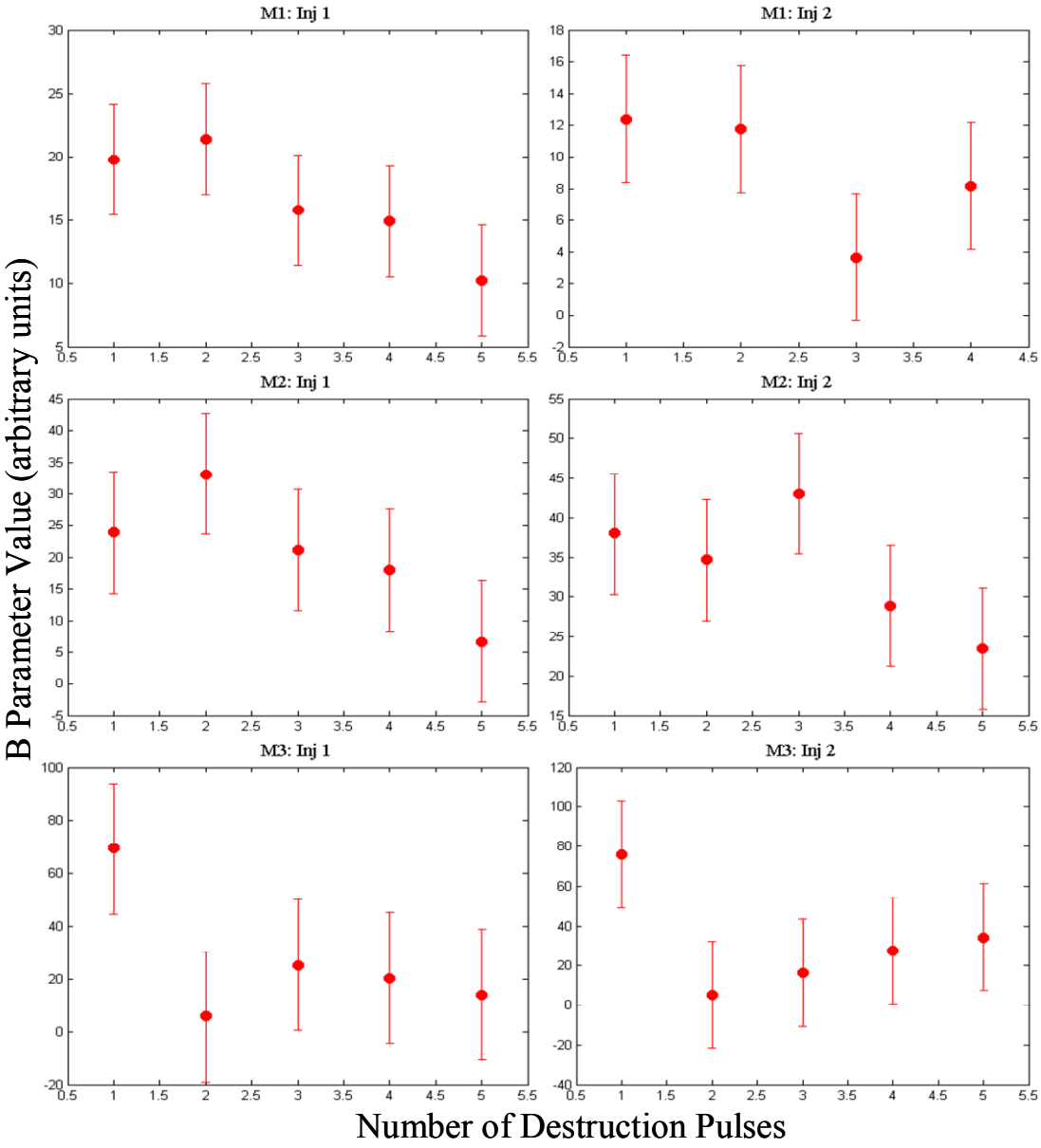

Figure 25. Five B measurements for each injection on mice 1-3. Error bars represent 1 standard deviation.

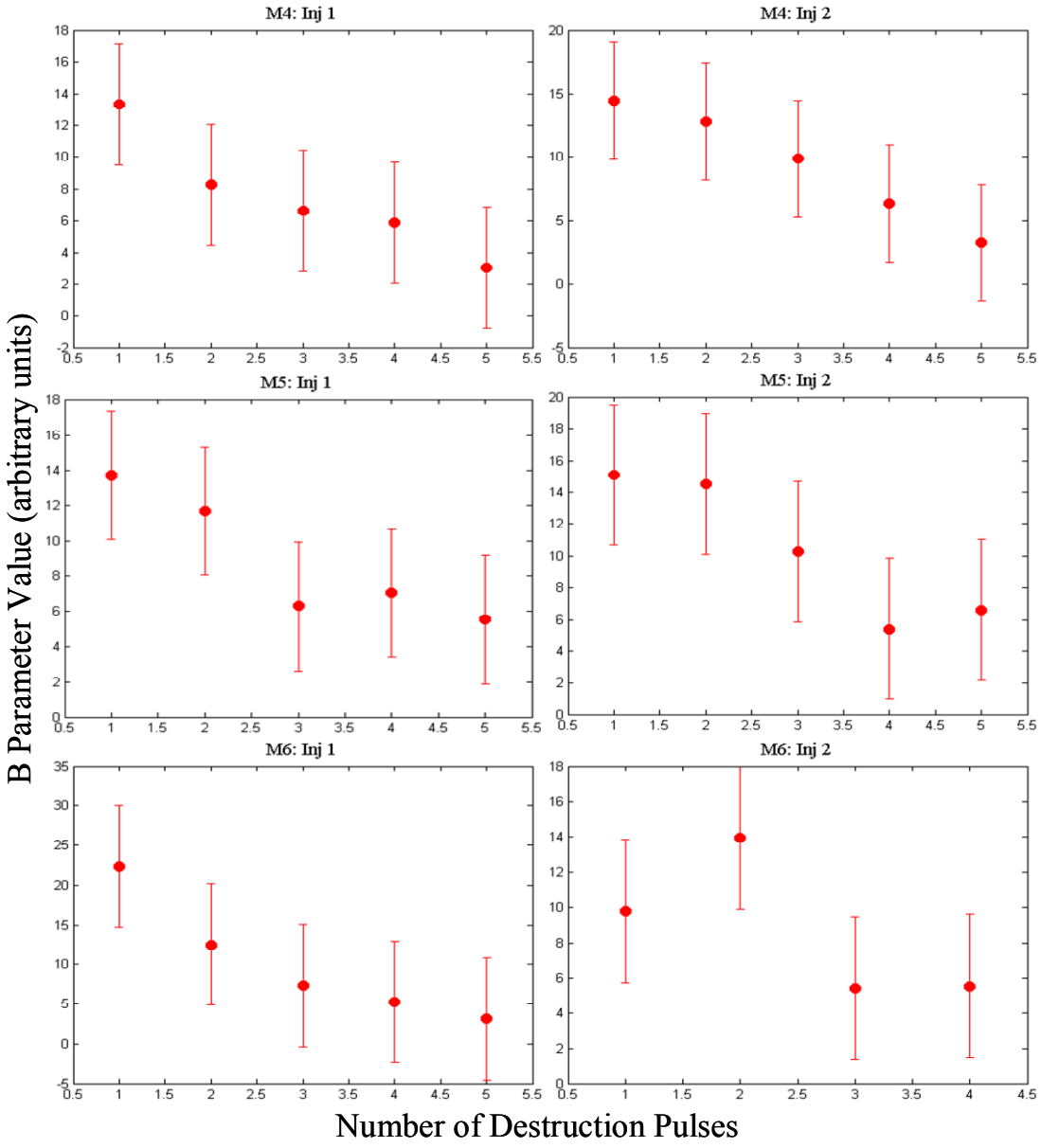

Figure 26. Five B measurements for each injection on mice 4-6. Error bars represent 1 standard deviation.

REFERENCES

1. King, J Roger. Cancer Biology 2nd ed. Harlow, England: Prentice Hall, 2000.

2. Hanahan D and RA Weinberg. *The hallmarks of cancer*. Cell 2000; 100(1): 57–70.

3. Kerbel R and J Folkman. *Clinical translation of angiogenesis inhibitors.* Nat Rev Cancer 2002; 2(10): 727–39.

4. Schlief R. *Development in echo-enhancing agents*. Clin Radiol 1996; 51(Supple 1): 5-7.

5. Ayida G, P Harris, S Kennedy, M Seif, D Barlow, P Chamberlain. *Hysterosalpingo-contrast sonography (Hy-CoSy) using Echovis-200 in the outpatient investigation of infertility patients.* Br J. Radiol 1996; 69(826): 910-913.

6. Quay SC. *Ultrasound contrast agent development: phast shift colloids.* J Ultrasound Med 1994; 13(Supple): S9.

7. Schneider M, M Arditi, MB Barrau, J Brochot, A Broillet, R Ventrone, F Yan. *BR1: a new ultrasonographic contrast agent based on sulfur hexachloride-filled microbubbles*. Invest Radiol 1995; 30(8): 451-457.

8. Bauer A, Mahler M, et al. *Microvascular imaging: results from a phase 1 study of the novel polmeric contrast agent SHU 563 A*. In: Nanda N N, Schlief R, et al Advances in echo imaging using contrast enhancement, 2nd edn. Lancaster, England: Kluwer; 1997:39-64.

9. J Bushberg, JA Seibert, EM Leidholdt Jr., JM Boone. The Essential Physics of Medical Imaging 2nd ed. Philedelphia, PA: Lippincott Williams & Wilkins: 2002.

10. McCulloch M, C Gresser, S Moos, J Odabashian, S Jaspar, J Bednarz P Burgess, D Carney, V Moore, E Sisk, A Waggoner, S Witt, D Adams. *Ultrasound Contrast Physics: A Series on Contrast Echocardiography*, Article 3. J of Am S of Echocard 2000; 13(10): 959-967.

11. Harvey CJ, MJ Blomley, RJ Eckersley, DO Cosgrove. *Developments in ultrasound contrast media.* Eur Radiol. 2001; 11(4): 675–689.

12. Schwarz KQ, GP Bezante, X Chen, D Phillips, R Schlief. *Hemodynamic effects of microbubble echo contrast*. J Am Soc Echocardiogr 1996; 9(6): 795–804.

13. Skyba DM, G Camarano, NC Goodman, RJ Price, TC Skalak, S Kaul. *Hemodynamic characteristics, myocardial kinetics and microvascular rheology of FS-069, a second-generation echocardiographic contrast agent capable of producing myocardial opacification from a venous injection.* J Am Coll Cardiol 1996; 28(1): 1292–1300.

14. Cosgrove D, R Eckersley, M Blomley, C Harvey. *Quantification of blood flow*. Eur Radiol 2001; 11(8): 1338-1344.

15. Yeh CK, MJ Yang, PC Li. *Contrast-specific ultrasonic flow measurements based on both input and output time intensities*. Ultrasound Med Biol 2003; 29(5): 671–678.

16. Krix M, F Kiessling, S Vosseler, I Kiessling, M Le-Huu, NE Fusenig, S Delorme. *Comparison of intermittent-bolus contrast imaging with conventional power Doppler sonography: quantification of tumour perfusion in small animals.* Ultrasound Med Biol 2003; 29(8): 1093–1103.

17. Wei K, AR Jayaweera, S Firoozan, A Linka, DM Skyba, S Kaul. *Quantification of myocardial blood flow with ultrasound-induced destruction of microbubbles administered as a constant venous infusion.* Circ. 1998; 97(5): 473-483.

18. Blomley MJ, T Albrecht, DO Cosgrove, JC Bamber. *Can relative contrast agent concentration be measured in vivo with color Doppler US?* letter on *Can relative contrast agent concentration be measured in vivo with color Doppler US?* Radiology 1997; 204(1): 279-281.

19. Kiessling F, S Greschus, MP Lichy, M Bock, C Fink, S Vosseler, J Moll, MM Mueller, NE Fusenig, H Traupe, W Semmler. *Volumetric computed tomography (VCT): a new technology for noninvasive, high-resolution monitoring of tumor angiogenesis.* Nat Med 2004; 10(10): 1133-8.

20. Evans DH,WN McDicken, R Skidmore, TP Woodcock. Doppler Ultrasound: Physics, Instrumentation and Clinical Applications 2nd ed. Chichester, England: John Wiley & Sons; 1989.

21. Lindner JR, PA Dayton, MP Coggins, K Ley, J Song, K Ferrara, S Kaul. *Noninvasive imaging of inflammation by ultrasound detection of phagocytosed microbubbles.* Circ. 2000; 102(5): 531-8.

22. O Lucidarme, Y Kono, J Corbeil, SH Choi, JL Golmard, J Varner, RF Mattrey. *Angiogenesis: Noninvasive quantitative assessment with contrast-enhanced functional US in murine model.* Radiology 2006; 239(3): 730 – 739.

23. Maes F, A Collignon, D Vandermeulen, G Marchal, P Suetens. *Multimodality image registration by maximization of mutual information*. IEEE Trans Med Imaging 1997; 16(2): 187-198.

24. Li R. Automatic placement of regions of interest in medical images using image registration, MS Thesis, Vanderbilt Univeristy, 2001.

25. Cosgrove, D. *Angiogenesis Imaging – Ultrasound*. The British Journal of Radiology 2003; 76(1): S43-S49.

26. Leong-Poi H, J Christiansen, AL Klibanov, S Kaul, JR Lindner. *Noninvasive assessment of angiogenesis by ultrasound and microbubbles targeted to α(v)-integrins*. Circ. 2003; 107(3): 455-60.

27. Lagalla R, G Caruso, R Urso, G Bizzini, L Marasa, V Miceli. The correlation between color Doppler using a contrast medium and the neoangiogenesis of small prostatic carcinomas. Radiol Med 200; 99(4): 270-275.

28. Bloch SH, PA Dayton, KW Ferrara. *Targeted imaging using ultrasound contrast agents.* IEEE Engineering in Medicine and Biology 2004; 23(5): 18-29.

29. Tofts PS. *Modeling tracer kinetics in dynamic Gd-DTPA MR imaging*. J. Magn. Reson. Imag. 1997; 7(1): 91–101.

30. Parker GJ, PS Tofts. *Pharmacokinetic analysis of neoplasms using contrast-enhanced dynamic magnetic resonance imaging.* Top.Magn. Reson. Imag. 1999; 10(2): 130–142.

31. Kruse DE, RH Silverman, RJ Fornaris, DJ Coleman, KW Ferrara, *A swept-scanning mode for estimation of blood velocity in the microvasculature*. IEEE Trans. Ultrason. Ferroelect. Freq. Contr. 1998; 45: 1437–1440.

32. Goertz DE, DA Christopher, JL Yu, RS Kerbel, PN Burns, FS Foster, *High-frequency color flow imaging of the microcirculation.* Ultrasound. Med. Biol. 2000; 26(1): 63–71.

33. Gillies RJ, N Raghunand, GS Karczmar, ZM Bhujwalla. *MRI of the tumor microenvironment*. J Magn Reson Imaging 2002; 16(4): 430-50.

34. Mikawa M, N Miwa, M Brautigam, T Akaike, A Maruyama. *Gd(3+)-loaded polyion complex for pH depiction with magnetic resonance imaging*. J Biomed Mater Res 2000; 49(3): 390–395.

35. Zhang S, K Wu, AD Sherry. *A novel pH-Sensitive MRI contrast agent.* Angewandte Chemie Int Ed 1999; 38(21): 3192–3194.

36. Li WP and CJ Anderson. *Imaging matrix metalloproteinase expression in tumors.* Q. J. Nucl. Med 2003; 47: 201–208.

37. Yeh CK, KW Ferrara, DE Kruse. *High-resolution functional vascular assessment with ultrasound.* IEEE Trans Med Imaging 2004; 23(10): 1263-75.

38. Bland JM, DG Altman. Statistical methods for assessing agreement between two methods of clinical measurement. *Lancet* 1986; 307-310.

39. Marret H, S Sauget, B Giraudeau, M Brewer, J Ranger-Moore, G Body, F Tranquart. *Contrast-enhanced sonography helps in discrimination of benign from malignant adnexal masses*. J Ultrasound Med 2004; 23(12): 1629-1639.

40. Korpanty G, JG Carbon, PA Grayburn, JB Fleming, RA Brekken. *Monitoring response to anticancer therapy by targeting microbubbles to tumor vasculature.* Clin Cancer Res 2007; 13(1): 323-330.